Thin-Film Organic Polymer Phototransistors

Michael C. Hamilton, *Student Member, IEEE*, Sandrine Martin, *Member, IEEE*, and Jerzy Kanicki, *Senior Member, IEEE*

***Abstract*—We have studied the electrical performance of organic polymer thin-film transistors (OP-TFTs) under steady-state white-light illumination, as well as the performance of these devices as photodetectors. The off-state drain current of the OP-TFT is significantly increased due to the illumination, while a smaller relative effect is observed on the drain current in the strong-accumulation regime. The illumination effectively decreases the threshold voltage of the device and increases the apparent subthreshold swing, while the field-effect mobility of the charge carriers in the polymer channel is unchanged. We have observed full recovery of our devices after the illumination is removed at room temperature. These observations are explained in terms of the photogeneration of excitons due to the absorbed photons. The photogenerated excitons subsequently diffuse and dissociate into free charge carriers, thereby enhancing the carrier density in the channel of the device. We have found broadband responsivities of approximately 0.7 mA/W for devices biased in the strong-accumulation regime and gate-to-source voltage-independent photosensitivities of approximately 10^3 for devices in the off-state. We also determine, for the first time, the flatband voltage of these devices to be about -2.3 V.**

***Index Terms*—Conjugated organic polymer, photodetector, photosensitivity, phototransistor, responsivity, thin-film transistor.**

I. Introduction

THIN-FILM transistors (TFTs) based on conjugated organic materials, both small-molecules and polymers, have shown promise for use in large-area low-cost applications [1], [2]. Several groups have proposed or reported successful integration of such devices with light-emitting devices to demonstrate the possibility of all-organic broad-area flat-panel displays. These applications include pentacene-based organic TFTs (OTFTs) integrated with organic light-emitting devices (OLEDs) [3], poly(hexylthiophene) (P3HT) based organic polymer TFTs (OP-TFTs) integrated with OLEDs [4], copper phthalocyanine (CuPc) based organic static induction transistors (SITs) that may be suitable for integration into display devices [5], OTFT- and OP-TFT-driven active-matrix polymer dispersed liquid-crystal displays (PD-LCDs) [6]–[8], and organic electrophosphorescent devices (OELDs) driven by all-organic pentacene-based OTFTs [9].

On the other hand, a number of other groups have described the use of polymer-based devices as photodetectors. These detectors can be classified into one of two main groups: the two-terminal photodiode and the three-terminal phototransistor. Several groups have discussed various organic photodiode structures [10]–[19]. The motivated reader will find useful reviews of recent work on organic photodetectors in [20]–[22]. A much smaller number of groups have published work on organic phototransistors, which is the subject of this paper. Zukawa *et al.* have demonstrated an organic heterojunction-based phototransistor [23]. Schön and Klock have shown the use of a pentacene-based metal–semiconductor field-effect transistor as a phototransistor [24]. Additionally, Narayan *et al.* have described an organic polymer field-effect transistor that responds to light [25], [26].

Since in optoelectronic applications, the device will either be integrated with light-emitting devices (as a switching device) or be used to detect light itself (as a light sensor), it is important to understand the effects of illumination on the electrical performance of these devices, as well as the underlying physics of these effects. In the past, our group has described the effect of white-light illumination on the electrical performance of amorphous silicon TFTs with a device structure similar to that described in this paper, and we have shown that these devices can function effectively as photosensors [27]. In this paper, we present the results of our investigation of the performance of our organic polymer TFTs under steady-state illumination from a broadband source and the performance of these devices as photodetectors.

II. Device Structure

A schematic cross-section of the device used in this study is shown in Fig. 1(a). The device is an inverted, defined-gate, gate-planarized, coplanar thin-film transistor that has been previously described [28]–[30]. Indium tin oxide (ITO) was used for the source and drain contacts. Benzocyclobutene (BCB) was used as the gate-planarization layer, and it also functions as a gate insulator. PECVD hydrogenated amorphous silicon nitride (a-SiN:H) was used as a second gate insulator layer, and chromium (Cr) was used for the patterned gate electrode. For the case of these devices, the usefulness of the BCB planarization layer is limited. However, if a thicker gate electrode is to be used, the planarization will allow for better step coverage of the subsequently deposited layers [31]. The devices were fabricated on a silicon substrate (with a thick thermally grown silicon dioxide layer) to facilitate processing in standard microelectronic fabrication equipment; however, this device structure could easily be fabricated on a glass substrate. We used a 1-wt % solution of the organic semiconductor F8T2 [poly(9, 9-dioctylfluorene-co-bithiophene)] alternating copolymer dissolved in either xylenes or mesitylenes. The polymer film was deposited by spin-coating and was cured in a vacuum oven at

Manuscript received December 5, 2003; revised March 22, 2004. This work was supported in part by the National Institute of Standards and Technology Advanced Technology Program and in part by the Department of Defense under a National Defense Science and Engineering Graduate Fellowship sponsored by the U.S. Air Force office of Scientific Research and administered by the American Society of Engineering Education. The review of this paper was arranged by Editor L. Lunardi.

The authors are with the Department of Electrical Engineering and Computer Science, The University of Michigan, Ann Arbor, MI 48109 USA (e-mail: kanicki@eecs.umich.edu).

Digital Object Identifier 10.1109/TED.2004.829619

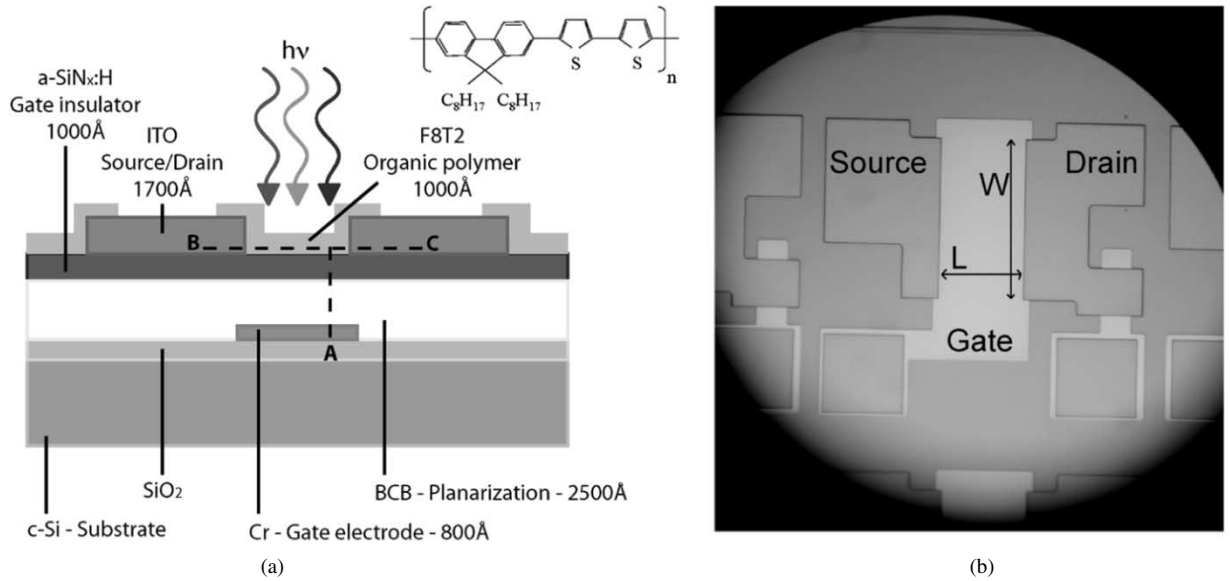

(a) (b)

Fig. 1. (a) Cross section of device structure and chemical structure of F8T2. (b) Top view of illuminated device showing gate, source, and drain. For this device, $L = 56\ \mu$m, $W = 116\ \mu$m, and source/drain-gate overlap is $5\ \mu$m.

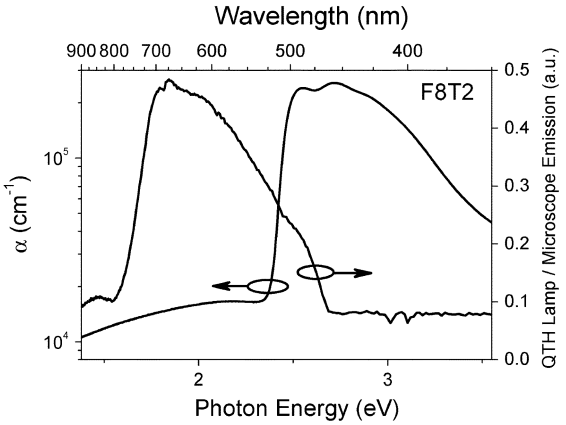

Fig. 2. Absorption coefficient of F8T2 and light emission spectrum of incident light as a function of the photon energy.

90 °C, providing a uniform and unpatterned film with an approximate thickness of 1000 Å. Samples are stored in air, at room temperature, and with yellow ambient light.

III. Experimental Setup

To investigate the effect of steady-state illumination on the electrical performance of our devices, the devices were illuminated from the top, as shown in Fig. 1(a). The experiments were carried out on a Karl Suss PM8 probe station, using broadband white light from a 150-W halogen lamp through a Mitutoyo microscope as the illumination source. The ultraviolet–visible absorption spectrum of a thin-film (1000 Å) of F8T2 on a quartz substrate (taken with a Cary 5e UV-Vis-NIR Spectrophotometer) and the spectrum of the incident light at the sample surface are shown in Fig. 2. From this figure, we can see that light from the lamp is absorbed mainly in the range of wavelengths from approximately 475–525 nm (2.6–2.4 eV). In this wavelength range, the absorption coefficient (α) varies from 2.5×10^5 to 2.5×10^4 cm^{-1}, providing a $1/\alpha$ light absorption depth from 400–4000 Å. Since the thickness of the F8T2 film is 1000 Å, we can conclude that the light intensity is relatively constant across the film, and we can assume that the irradiance inside the polymer film at the channel is approximately equal to the irradiance at the film surface (i.e., the photons are uniformly absorbed throughout the polymer film). The incident light irradiance at the surface of the film, measured using an International Light SED625 thermopile detector connected to an International Light IL1700 research radiometer, was controlled from 0–2.9 W/cm^2. The light delivered to the device was focused to a spot size approximately equal to the area of the device, and the entire channel of the device was illuminated as shown in Fig. 1(b).

We measured the OP-TFT electrical characteristics in the dark and under various levels of illumination at room temperature using an HP4156 semiconductor parameter analyzer controlled by Interactive Characterization Software (Metrics). The bias conditions used to measure the transfer characteristics (in both the linear and saturation regimes) and the output characteristics of our devices are given in Table I. We chose to measure the transfer characteristics from the on-state to the off-state (i.e., from $V_{\rm GS} = -40$ to 20 V), as shown in Table I. This measurement method was chosen because it provides very reproducible data, with a variation in the on-current of less than $\pm 5\%$ for the linear regime transfer characteristics measured back-to-back in the dark. This allows reliable comparison of the electrical performance of the device in the dark and under illumination.

IV. Device Operation

A. In the Dark

OP-TFTs based on F8T2 exhibit p-channel field-effect transistor behavior (i.e., holes are accumulated within the channel), as can be seen from the dark output characteristics (drain current versus drain-to-source voltage, $I_D - V_{\rm DS}$) shown in Fig. 3(a). As expected, for field-effect transistors, the output characteristics show two distinct regions of device

TABLE I
OP-TFT ELECTRICAL CHARACTERISTICS MEASUREMENT BIAS CONDITIONS

Transfer Characteristics		
V_G	Initial	$-40V$
	Final	$20V$
	Step	$+1V$
V_D	Linear	$-5Vor-10V$
	Saturation	V_G
V_S	Common	$0V$
Output Characteristics		
V_G	$-40, -30, -20, -10V$	
V_D	Initial	$0V$
	Final	$-40V$
	Step	$-1V$
V_S	Common	$0V$

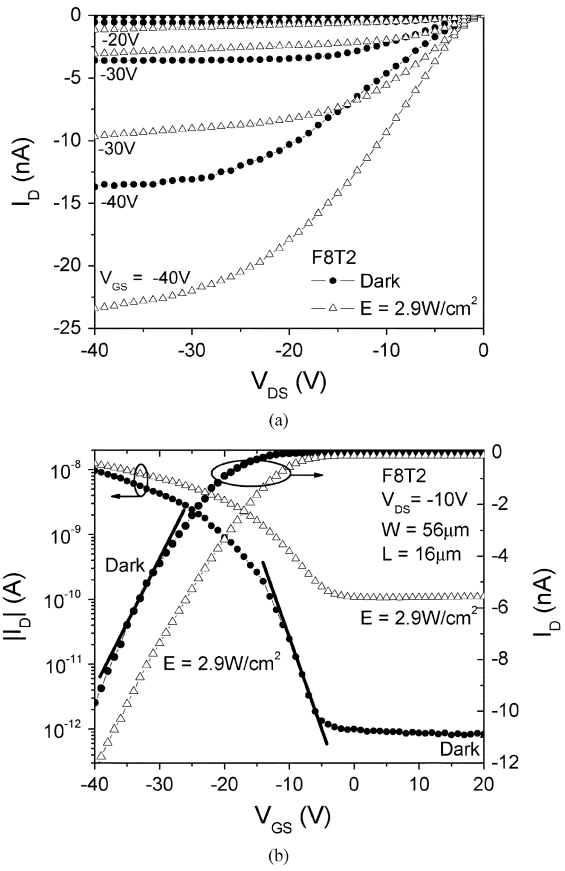

Fig. 3. (a) Output characteristics of OP-TFT in the dark and illuminated at 2.9 W/cm^2. (b) Transfer characteristics of OP-TFT in the dark and illuminated at 2.9 W/cm^2.

operation: linear and saturation. The nonideal behavior of the device in the linear regime (at low $V_{\rm DS}$) is most likely due to the current crowding associated with the contact resistance between the polymer channel and the source and drain electrodes [32]. The linear regime transfer characteristics (drain current versus gate-to-source voltage, $I_D - V_{GS}$) of a typical device in the dark are presented in Fig. 3(b). In this paper, we extract the linear regime field-effect mobility and threshold voltage from the linear regime transfer characteristics using the following equation, based on the MOSFET gradual channel approximation [33]:

$$I_D = -\mu_{\rm FElin} C_{\rm ins} \frac{W}{L}\left[(V_{\rm GS} - V_T)V_{\rm DS} - \frac{V_{\rm DS}^2}{2}\right] \quad (1)$$

or for low $V_{\rm DS}$

$$I_D = -\mu_{\rm FElin} C_{\rm ins} \frac{W}{L}(V_{\rm GS} - V_T)V_{\rm DS}. \quad (2)$$

In these equations, $\mu_{\rm FElin}$ is the linear regime field-effect mobility [square centimeters per volt per second (cm^2/V $\cdot$ s)], $C_{\rm ins}$ is the gate insulator capacitance per unit area [Farad per square centimeter (F/cm^2)], W is the channel width of the device, L is the channel length of the device, $V_{\rm GS}$ is the applied gate-to-source bias, $V_{\rm DS}$ is the applied drain-to-source bias, and $V_{T\rm lin}$ is the linear regime threshold voltage given by the following for MOSFETs [34]:

$$V_{T\rm lin} = 2\phi_F - \frac{\epsilon_{\rm semi}}{\epsilon_{\rm ins}} d_{\rm ins}\sqrt{\frac{4qN_A^{\rm eff}}{\epsilon_{\rm semi}\epsilon_{\rm ins}}(-\phi_F)} + V_{\rm FB}^{\rm eff} \quad (3a)$$

$$V_{\rm FB}^{\rm eff} = \phi_{\rm MS} - \frac{Q_{\rm eff}}{C_{\rm ins}}. \quad (3b)$$

Here, ϕ_F is the electrostatic potential in the semiconductor bulk, $\epsilon_{\rm semi}$ and $\epsilon_{\rm ins}$ are the dielectric constants of the semiconductor and insulator, respectively, $d_{\rm ins}$ is the effective thickness of the insulator, $N_A^{\rm eff}$ is the effective acceptor density, $\phi_{\rm MS}$ is the potential difference between the metal gate and semiconductor bulk at zero gate bias, and $Q_{\rm eff}$ is the effective interface charge. For simplicity, we account for the cumulative effect of all charges, other than that from $N_A^{\rm eff}$, in the semiconductor by assuming an effective charge $Q_{\rm eff}$ at the semiconductor-to-gate insulator interface [35]. In actuality, the charges in the device that affect the threshold voltage of OP-TFTs are the fixed bulk charge, the mobile charge, and the interface trapped charge. We associate the negative threshold voltage of the p-channel OP-TFTs with the density of positively charged states in the semiconductor channel N_T [36].

The subthreshold swing was extracted from the linear regime transfer characteristics, in the transition from the off-state to the on-state, using the following equation:

$$I_D \propto 10^{-V_{\rm GS}/S}. \quad (4)$$

In this equation, S is the subthreshold swing (volts per decade), which can be associated with the density of deep bulk states ($N_{\rm BS}$) in the organic semiconductor and interface states ($N_{\rm SS}$) at the interface between the gate insulator and organic semiconductor through [37]

$$S = \frac{kT}{q\log(e)}\left[1 + \frac{qd_{\rm ins}}{\epsilon_{\rm ins}}(\sqrt{\epsilon_{\rm semi}N_{BS}} + qN_{\rm SS})\right] \quad (5)$$

where k, k, and q are the usual physical parameters, and $\epsilon_{\rm ins}$, $\epsilon_{\rm semi}$, and $d_{\rm ins}$ have been described above. It should be noted that (5) was developed for a-Si:H TFTs, and a relation between the subthreshold swing of an OP-TFT and the density of states

in the active organic semiconductor material has yet to be developed. However, we can assume that the subthreshold swing can be positively associated with the densities of bulk states and interface states (i.e., as the state densities increase, the device will turn on slower with applied gate bias, and therefore a larger subthreshold swing will be observed). This agrees with the relation shown in (5).

From the linear regime transfer characteristics of a device in the dark, shown in Fig. 3(b), we find values of the linear regime field-effect mobility, threshold voltage, and subthreshold swing to be $4\times10^{-3}\text{cm}^2/\text{V}\cdot\text{s}$, -25 V, and 3.0 V/decade, respectively.

The saturation regime field-effect mobility (μ_{FEsat}) and threshold voltage ($V_{T\text{sat}}$) were extracted from the saturation regime transfer characteristics (drain current versus gate-to-source voltage $I_D - V_{\text{GS}}$ with $V_{\text{DS}} = V_{\text{GS}}$ for the saturation regime) using the following equation, based on the MOSFET theory [33]:

$$I_D = -\mu_{\text{FE sat}} C_{\text{ins}} \frac{W}{2L}(V_{\text{GS}} - V_T)^2. \tag{6}$$

From the saturation regime transfer characteristics (as can be found in [28]), we find values of the saturation regime field-effect mobility and threshold voltage to be $3 \times 10^{-3}\text{cm}^2/\text{V}\cdot\text{s}$ and -20 V, respectively.

B. Under Illumination

We have observed very strong effects of steady-state broadband illumination on the electrical performance of OP-TFTs. The effects are evident when we compare the linear regime transfer characteristics of a device in the dark to those of the same device under illumination as shown in Fig. 3(b). From this figure, we can see that the drain current in the off-state is significantly increased by several orders of magnitude, while a milder effect of illumination on the drain current in the strong-accumulation regime is observed. The significant increase of drain current in the off-state, when the device is under illumination, can be attributed to the enhancement of the carrier density in, and therefore the conductivity of, the channel of the device due to the photogeneration of excitons in the polymer.

The following are the four basic photocarrier generation processes in solid organic polymers that can contribute to the enhancement of the carrier density in the polymer channel of the device [38]:

1) exciton formation and subsequent dissociation (electric field, surface, or impurity induced) into free carriers;
2) direct, band-to-band excitation of electrons;
3) photoinjection of carriers from the metal source/drain electrodes into the polymer;
4) detrapping of carriers trapped in localized gap states in the polymer.

For the case of our devices, the most likely carrier photogeneration process is through the exciton route. Photons with the proper energy are absorbed in the polymer, forming an exciton (i.e., a bound electron-hole pair) as shown schematically in Fig. 4(a) and (b). This exciton diffuses to a dissociation site (i.e., defect, impurity, or surface state) and dissociates into an electron and hole. Once generated, these charge carriers begin to move under the influence of the electric field (from the applied V_{DS} and V_{GS}) and in opposite directions down the channel

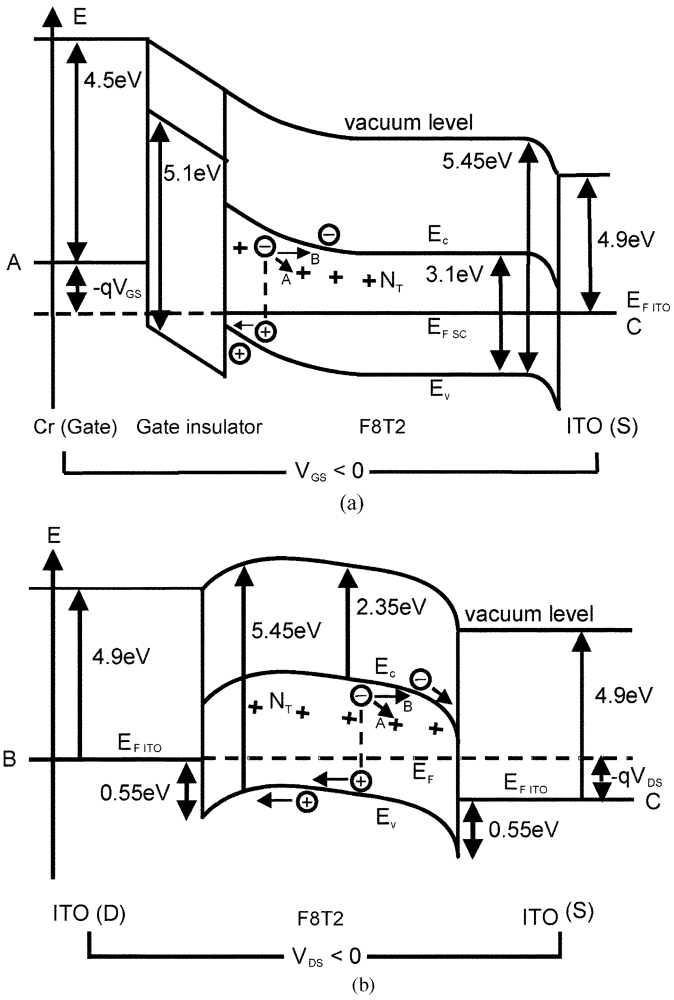

Fig. 4. Proposed energy band diagram of OP-TFT under illumination in the region from (a) the gate electrode to the source electrode [i.e., following the line A to C in Fig. 1(a)] and (b) the drain electrode to the source electrode [i.e., following the line B to C in Fig. 1(a)].

of the OP-TFT. With our biasing conditions, the electrons move away from the gate and drain and toward the source, while the holes move toward the gate and drain and away from the source. Some of the photogenerated electrons are trapped into and neutralize positively charged states (N_T) that contribute to the large initial negative threshold voltage, thereby reducing the threshold voltage. The origin of these positively charged states is presently under investigation. The photogenerated holes are collected at the drain electrode (by the corresponding transfer of an electron from the drain electrode into the valence band of the polymer). A photocurrent is measured that is larger than the drain current in the dark, especially when the device is operated in the off-state. These processes are shown schematically in the proposed energy band diagrams presented in Fig. 4(a) and (b). Fig. 4(a) shows the energy band diagram of a device under illumination, normal to the channel of the device (i.e., in the direction from the gate, through the gate insulator, and through the semiconductor) near the source electrode. Fig. 4(b) shows the energy band diagram of a device under illumination, in the direction of the channel of the device (i.e., in the direction from the drain electrode, through the semiconductor, to the source electrode). When the device is operated in the strong-accumulation regime,

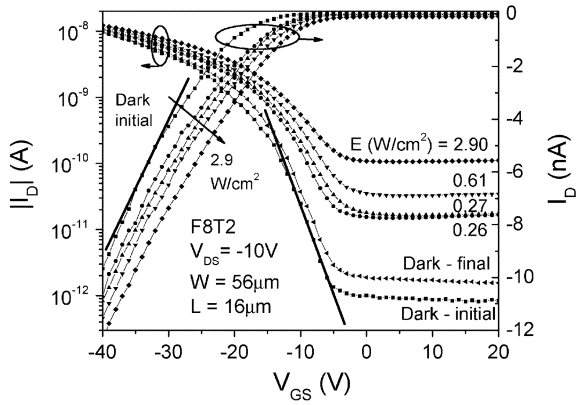

Fig. 5. Transfer characteristics of OP-TFT in the dark and under various irradiance levels.

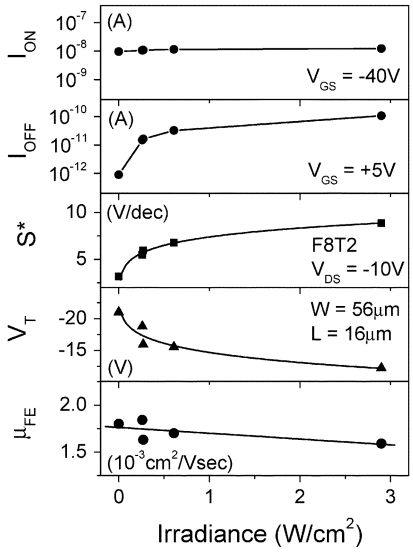

Fig. 6. Dependence of on-state drain current, off-state drain current, field-effect mobility, threshold voltage, and apparent subthreshold slope on irradiance. $\mu_{\rm FE}$, V_T, and S^* extracted from the data in Fig. 5, using (2) and (4). Lines are provided as guides to the eye.

the relative effect of illumination on the drain current is much smaller compared to the effect in the off-state. This effect can be explained by the overwhelming effect of the gate voltage on the concentration of accumulated carriers in the channel of the device, at the levels of illumination used in this study, and is explained in further detail below.

V. Experimental Results

We have investigated the effect of the illumination irradiance level. Fig. 5 presents the linear regime transfer characteristics of our OP-TFT in the dark and under various levels of illumination up to approximately 2.9 W/cm^2. From this figure, we can see that the off-state drain current of the device is strongly dependent on the level of illumination. As the illumination level is increased, the drain current is increased, since the photogeneration rate of excitons (and therefore charge carriers) in the channel of the device increases as the illumination intensity is increased.

Fig. 6 presents the variation of the off-state drain current, on-state drain current, linear regime field-effect mobility, threshold voltage, and apparent subthreshold swing (S^*) with

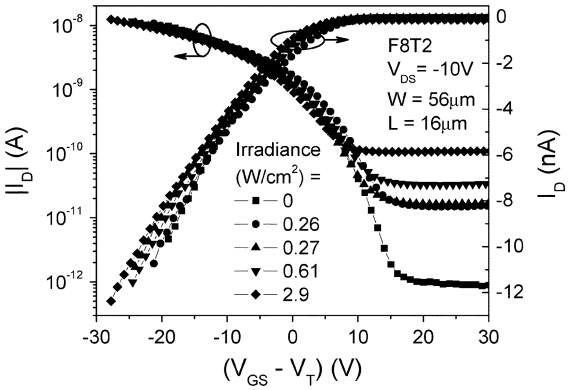

Fig. 7. Threshold voltage-normalized transfer characteristics (i.e., I_D versus $V_{\rm GS} - V_T$) of OP-TFT in the dark and illuminated at various irradiance levels.

illumination irradiance. From this figure, we see that the relative change in the off-state drain current, as the irradiance level is increased, is much larger than the relative change in the on-state drain current, as stated above. The other electrical parameters were extracted from the linear regime transfer characteristics of Fig. 5 using (2) and (4). From Fig. 6, it is evident that as the illumination level is increased, the threshold voltage of the device is effectively reduced, and the apparent subthreshold swing is increased. We speculate that the reduction of the threshold voltage is due to the compensation of positively charged states (N_T, which contribute to the large initial negative threshold voltage) by the photogenerated electrons (i.e., the electrons are trapped by positively charged states). This effect can be understood by examining (3a) and (3b) for the threshold voltage of a MOSFET. If we use this equation to explain the behavior of OP-TFTs under illumination, we see that a reduction of N_T corresponds to a reduction of $Q_{\rm eff}$, which leads to a reduction of the threshold voltage. In Fig. 7, we present the transfer characteristics plotted using the effective gate-to-source voltage (i.e., I_D versus $V_{\rm GS} - V_T$) at various illumination levels. From this figure, we can see that, indeed, the major effect of the illumination is a reduction of the threshold voltage. Conversely, the field-effect mobility is relatively unaffected, indicating that the electronic structure of the polymer is not affected by the illumination. Additionally, we conclude that there is negligible change in temperature due to illumination of the device, since the field-effect mobility is expected to increase with temperature in conjugated polymer semiconductors [39]–[41]. The apparent increase in the subthreshold swing with increasing illumination can be attributed to the enhanced conductivity of the channel of the device in the off-state due to the increase in carrier density brought about by the illumination. This is an additive effect, in that the illumination provides another means by which to control the density of charge carriers in the channel and can be thought of as a second gate. When either of the gates is turned off (i.e., $V_{\rm GS} \geq 0$ V applied or no incident illumination), the effect of the other gate is maximized. For instance, the on/off ratio $(I_{\rm on}/I_{\rm off})$ is maximum for no illumination, and $I_{D\rm illum}/I_{D\rm dark}$ is maximum for a device biased in the off-state. The observed result is an apparent decrease in the effectiveness of the applied gate bias over the channel (i.e., larger apparent subthreshold swing). However, as shown in Fig. 7, we see that the subthreshold swing

of all curves, dark and illuminated, is similar. The increase in the apparent subthreshold swing is an artifact of the extraction method using (4) under illumination. Using the relation of (5), the density of states can be connected to the subthreshold swing and can be extracted from the transfer characteristics in the dark and under illumination. From Fig. 7, we conclude that since the subthreshold swing is not significantly affected by the illumination, the density of states in the polymer is not significantly affected by the illumination.

Alternatively, the observed results can be understood by investigating the band-bending and energy level structure in the organic semiconductor in the direction normal to the channel of the device. This theory has been developed for TFTs based on inorganic materials, namely hydrogenated amorphous silicon (a-Si:H) TFTs [42]–[44]. The nonequilibrium situation of the illuminated device is characterized by a splitting of the equilibrium Fermi level into two quasi-Fermi levels: one for holes and one for electrons. The splitting is dependent on the intensity and energy of the incident illumination. The band-bending (i.e., the effect the gate has on the accumulated carrier concentration in the channel), at a certain gate bias, is reduced in the illuminated device due to the increased density of charge carriers in the channel from photogeneration. Experimentally, we observe this effect as a reduction in the threshold voltage and an increase in the apparent subthreshold swing.

A useful figure of merit is the responsivity (R in amperes per watt) of the device, which can be defined as

$$R = \frac{I_{\rm ph}}{P_{\rm inc}} = \frac{(I_{D\rm illum} - I_{D\rm dark}) \times A}{E} \tag{7}$$

where $I_{\rm ph}$ is the drain photocurrent, $P_{\rm inc}$ is the power incident on the channel of the device, $I_{D\rm illum}$ is the drain current under illumination, $I_{D\rm dark}$ is the drain current in the dark, E is the irradiance of the incident light, A is the effective device area, and the other parameters have been described above. The effective device area A is calculated from the geometry of the device. A is equal to the effective channel length $L + 2L_p$ times the effective channel width $W + 2L_p$, where L_p is the diffusion length of the holes. For $L_p \ll L, W$, which is the case here (i.e., 100 nm $\ll$ 6000 nm), the equation reduces to $L \times W$. A plot of R versus gate bias is shown in Fig. 8. From this plot, we observe that the responsivity is higher in the strong-accumulation regime than in the off-state. This is evidence of a gain mechanism in the device, since the number of photogenerated carriers mostly depends on the intensity of the incident illumination , and not on the applied gate bias. We have observed values of R in excess of 0.7 mA/W for the case of broadband illumination. This value is several orders of magnitude lower than reported responsivities of 0.1–0.5 A/W of other organic photodetectors under monochromatic illumination [11], [13]. However, the responsivity of the present devices is expected to be significantly larger for a monochromatic light source having a photon energy corresponding to the maximum absorption of the polymer as compared to the present case in which most of the incident light is not absorbed [45], [46]. In Fig. 9, we present the dependence of the responsivity on the illumination irradiance. We can see from this figure that the device has the highest responsivity when biased in the strong-accumulation regime, and the responsivity decreases with increasing irradiance. The decrease of responsivity as irradiance is increased is due to the saturation of the photocurrent, which can be caused by several factors. One factor influencing the photocurrent is the efficiency of charge transport through the channel of the device at higher irradiance levels. In other words, even though more excitons and, therefore, more holes are photogenerated at higher irradiance levels, these carriers may not be able to contribute to the photocurrent due to the limiting nature of the charge transport mechanisms, such as space-charge-limited currents, in the polymer. A second cause of the photocurrent saturation at higher irradiance levels is exciton–exciton annihilation (i.e., at higher irradiance levels, the enhanced density of excitons causes the excitons to interact with each other).

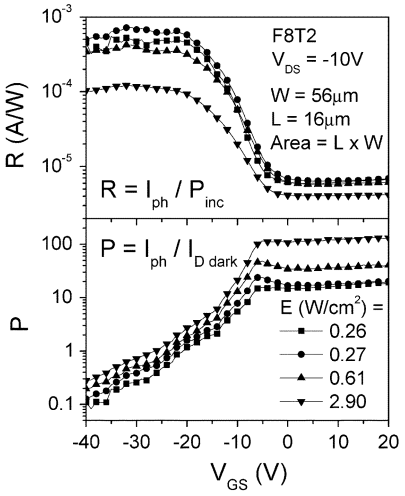

Fig. 8. OP-TFT responsivity R and photosensitivity P versus $V_{\rm GS}$ for various irradiance levels [extracted from the data in Fig. 4 using (7) and (8)].

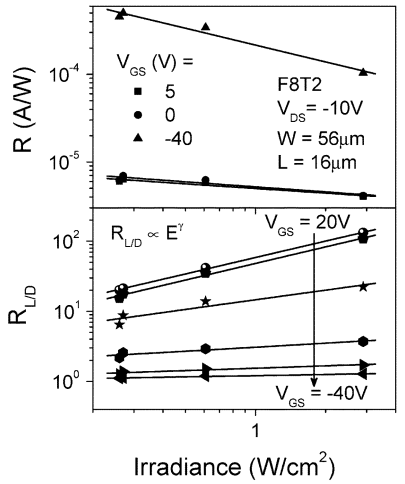

Fig. 9. OP-TFT responsivity R and photoresponse $R_{L/D}$ versus irradiance for various $V_{\rm GS}$.

A second useful figure of merit is the photosensitivity P, or signal (photocurrent) to noise (dark-current) ratio, of the device, which is defined as [47]

$$P = \frac{\text{signal}}{\text{noise}} = \frac{I_{\rm ph}}{I_{D\rm dark}} = \frac{(I_{D\rm illum} - I_{D\rm dark})}{I_{D\rm dark}} \tag{8}$$

where all terms have been previously defined. The dependence of the photosensitivity on the gate voltage $V_{\rm GS}$ is shown in

Fig. 8. From this plot, we can see that P is a maximum in the off-state and is minimum in the strong-accumulation regime, consistent with the observations and comments made above about the drain current under illumination. We have observed values of P in excess of 10^3 in the off-state at a broadband illumination level of 2.9 W/cm^2. From Fig. 8, we can also see that P is not a strong function of $V_{\rm GS}$ in the off-state. In fact, the slight dependence on $V_{\rm GS}$ and the little noise of the $P - V_{\rm GS}$ curve are mainly due to the extremely low ($< 10^{-12}$ A) off-state drain current of our OP-TFTs in the dark. The high sensitivity to illumination and nondependence on the gate-to-source bias in the off-state are very useful characteristics of the device if it is to be used to detect light at low applied voltages (i.e., low power consumption). Fig. 8 also shows the dependence of the photosensitivity on $V_{\rm GS}$ for several values of illumination irradiance. We can see that (as expected) P increases with increasing illumination irradiance. However, the photosensitivity for a device biased in the off-state is nearly linear with the irradiance level, giving a limited dynamic range that may not be very satisfactory for certain detector applications.

A related measure is the ratio of total drain current under illumination to drain current in the dark, which is referred to as the photoresponse and is defined as [27]

$$R_{L/D} = \frac{I_{D\rm illum}}{I_{D\rm dark}}. \tag{9}$$

A plot of $R_{L/D}$ versus E for various $V_{\rm GS}$, as shown in Fig. 9, shows that $R_{L/D}$ exhibits a power law dependence on the illumination according to the following equation:

$$R_{L/D} \propto E^{\gamma}. \tag{10}$$

In this equation, E is the illumination irradiance, and the γ-power exponent is a function of the applied $V_{\rm GS}$. We can describe the dependence of γ on $V_{\rm GS}$, as shown in Fig. 10, using a model that was developed by Harm *et al.* for hydrogenated amorphous silicon (a-Si:H) TFTs [42], [43], [48]. This model was formulated with the assumption that: 1) the total density of states is constant around midgap; 2) there is a symmetrical overlap of donor and acceptor states around midgap; 3) the field-effect is governed by the bulk states, as opposed to the interface states; and 4) under illumination, the Fermi level splits into quasi-Fermi levels (one for holes and one for electrons). We believe that these assumptions are not too specific to a-Si; therefore, we have applied this model to the case of OP-TFTs under illumination. The dependence of γ on $V_{\rm GS}$, as shown in Fig. 10, can be modeled by the following equations:

$$\gamma(V_{\rm GS}) = \begin{cases} \gamma_0 \left(1 - \frac{(V_{\rm GS} - V_{\rm FB})}{V_{\rm GC}}\right), & \text{for } V_{\rm GS} < V_{\rm FB} \quad \text{(11a)} \\ \gamma_0, & \text{for } V_{\rm GS} > V_{\rm FB}. \quad \text{(11b)} \end{cases}$$

In this equation, γ_0 is a material-dependent constant, $V_{\rm GS}$ is the applied gate-to-source bias, $V_{\rm FB}$ is the flatband voltage (i.e., the gate voltage necessary to achieve the flatband condition), and $V_{\rm GC}$ is the critical gate voltage at which the drain current under illumination is ideally equal to the drain current in the dark (i.e., $I_{D\rm illum}/I_{D\rm dark} = 1$ at $V_{\rm GC}$ for the ideal case) and is given by

$$V_{\rm GC} = \frac{\sqrt{\epsilon_{\rm semi}} d_{\rm ins} \beta}{\epsilon_{\rm ins}\sqrt{\epsilon_0}}. \tag{12}$$

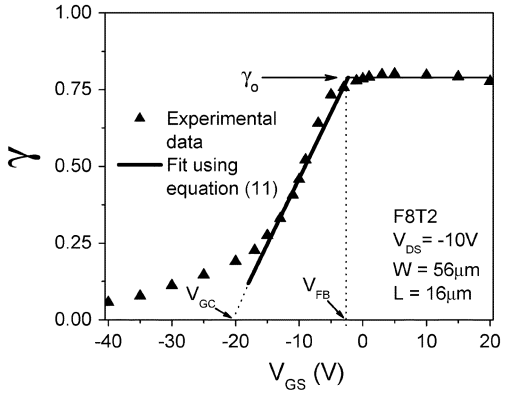

Fig. 10. γ [experimental and fit using (11a) and (11b)] versus $V_{\rm GS}$.

In this equation, $\epsilon_{\rm semi}$ is the dielectric constant of the semiconductor (=2.6), $\epsilon_{\rm ins}$ is the effective dielectric constant of the insulator (=2.3), $d_{\rm ins}$ is the effective thickness of the insulator (=2700 Å), and β is defined as

$$\beta = \frac{(2N_f)^{3/2}}{L} \tag{13}$$

where L is the linear slope of the localized state distribution near the middle of the supposed bandgap, and $2N_f$ is the total density of states at midgap. In Fig. 10, we see that we can fit our data in the region $0 < |V_{\rm GS}| < V_{\rm GC}$ using (11a) with $V_{\rm GC}$ equal to approximately -21 V. This gives a β value of approximately 7.4×10^5. If we assume a value of 10^{18} cm$^{-3} \cdot$ eV^{-1} for $2N_f$ (estimated from (5) with $N_{\rm SS} = 0$), we find that L is equal to 1.4×10^{21} cm$^{-3} \cdot$ eV^{-2} from (13). From experimental data, we estimate γ_0 to be 0.8, while the fit using (11b) gives a γ_0 value of approximately 0.9. A power-law dependence on the illumination irradiance is expected when trapping and subsequent detrapping, i.e., multistep hopping, of the carriers are involved in the channel conduction process.

Using a method similar to that of Schropp *et al.* [42], [43], we can extract the flatband voltage $V_{\rm FB}$ of the OP-TFTs from Fig. 10. Since the density of holes in the channel does not increase for applied gate biases from the flatband voltage to more positive voltages and the source and drain electrodes block electrons coming from the conduction band (i.e., lowest unoccupied molecular orbital, or LUMO level), the ratio of drain current under illumination over drain current in the dark is constant for positive gate voltages. As gate biases from the flatband voltage to more negative biases are applied, the logarithm of the current ratio is approximately proportional to the band-bending at the interface, which is proportional to $V_{\rm GS} - V_{\rm FB}$. As did Schropp *et al.*, we assume that the illumination does not cause a shift in the flatband voltage, and we extract the flatband voltage from the crossing point of (11a) and (11b). We find the $V_{\rm FB}$ of OP-TFTs based on F8T2 to be equal to -2.3 V.

In Fig. 11, we present the ratio of drain current under illumination to drain current in the dark versus $V_{\rm DS}$ at several values of $V_{\rm GS}$ spanning the entire range of operating regimes of the device. From this figure, we can see that this ratio is relatively independent of $V_{\rm DS}$, in the range of biases we have measured. The nondependence on $V_{\rm DS}$ shows that this range of electric fields is substantial to aid the dissociation of the excitons into free carriers.

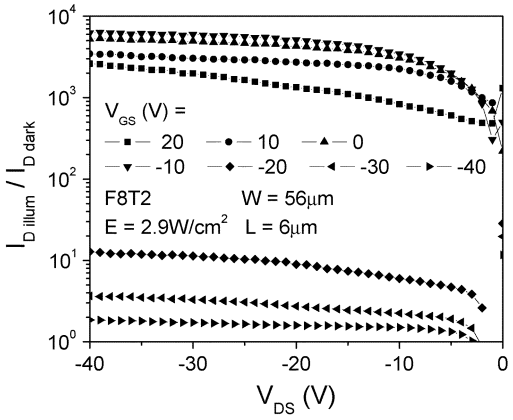

Fig. 11. $I_{D\mathrm{illum}}/I_{D\mathrm{dark}}$ at maximum irradiance versus V_{DS} at various V_{GS}.

It should be noted that the devices undergo full recovery, at room temperature, and relax back to their original state (i.e., off-state drain current, threshold voltage, and subthreshold swing values equal to preillumination values) after the illumination is removed. This effect can be seen in Fig. 5 where $I_{D\mathrm{final}}$ has nearly returned to $I_{D\mathrm{initial}}$. This recovery takes several minutes, in some cases, when the device is in the air at room temperature. However, exposing the device to higher temperature or illumination at longer wavelengths (i.e., red to infrared) can accelerate the recovery process [49].

VI. Conclusion

We have studied the electrical performance of F8T2-based OP-TFTs under white-light illumination and the performance of these devices as photodetectors. We have shown that the off-state drain current of the device is significantly increased due to the illumination, while a smaller relative effect is observed on the drain current in the strong-accumulation regime. As the illumination irradiance level is increased from 0 to 2.9 W/cm^2, the threshold voltage decreases by almost 10 V, while the field-effect mobility is unaffected. We also shown that the subthreshold swing of the transfer characteristics (and therefore the density of states of the polymer) is unchanged by illumination of the device. We observe full recovery of these devices (at room temperature) after the illumination is removed. These effects are explained by the photogeneration of excitons in the polymer. The excitons diffuse to dissociation sites and subsequently dissociate into free charge carriers, electrons, and holes, which move under the influence of the source-to-drain electric field. The electrons are trapped into positively charged states, thereby reducing the threshold voltage. The excess holes are collected at the drain electrode, increasing the drain current.

The effects of the broadband illumination irradiance level on the responsivity R, photosensitivity P, and photoresponse $R_{L/D}$ of these devices have also been presented. The responsivity for a device biased in the strong-accumulation regime is found to be approximately 0.7 mA/W, and the gate-to-source voltage-independent photosensitivity for a device in the off-state is found to be near 10^3 for broadband irradiance levels on the order of 1 W/cm^2. Using a method that has been developed for a-Si:H TFTs, we find the flatband voltage (V_{FB}) of these devices to be -2.3 V.

Acknowledgment

The authors would like to thank The Dow Chemical Company for the organic polymer (F8T2) used in this research. The authors also acknowledge Dr. J. Y. Nahm for the fabrication of the active substrates used in this work.

References

[1] G. Horowitz, "Organic field-effect transistors," *Adv. Mater.*, vol. 10, pp. 365–377, 1998.
[2] C. D. Dimitrakopoulos and D. J. Mascaro, "Organic thin-film transistors: A review of recent advances," *IBM J. Res. Dev.*, vol. 45, pp. 11–27, 2001.
[3] T. N. Jackson, Y. Lin, D. J. Gundlach, and H. Klauk, "Organic thin-film transistors for organic light-emitting flat-panel display backplanes," *IEEE J. Select. Topics Quantum Electron.*, vol. 4, pp. 100–104, Jan.–Feb. 1998.
[4] H. Sirringhaus, N. Tessler, and R. H. Friend, "Integrated optoelectronic devices based on conjugated polymers," *Science*, vol. 280, pp. 1741–1743, 1998.
[5] K. Kudo, D. X. Wang, M. Iizuka, S. Kuniyoshi, and K. Tanaka, "Organic static induction transistor for display devices," *Synth. Met.*, vol. 111–112, pp. 11–14, 2000.
[6] C. D. Sheraw, L. Zhou, J. R. Huang, D. J. Gundlach, T. N. Jackson, M. G. Kane, I. G. Hill, M. S. Hammond, J. Campi, B. K. Greening, J. Francl, and J. West, "Organic thin-film transistor-driven polymer-dispersed liquid crystal displays on flexible polymeric substrates," *Appl. Phys. Lett.*, vol. 80, pp. 1088–1090, 2002.
[7] H. E. A. Huitema, G. H. Gelinck, J. B. P. H. van der Putten, K. E. Kuijk, C. M. Hart, E. Cantatore, P. T. Herwig, A. J. J. M. van Breemen, and D. M. de LeeuW, "Plastic transistors in active-matrix displays," *Nature*, vol. 414, p. 599, 2001.
[8] H. E. A. Huitema, G. H. Gelinck, J. B. P. H. van der Putten, E. Cantatore, K. E. Kuijk, C. M. Hart, and D. M. de LeeuW, "Polymer-based transistors used as pixel switches in active-matrix displays," *J. SID*, vol. 10, pp. 195–202, 2002.
[9] S. W. Pyo, Y. M. Kim, J. H. Kim, J. H. Shim, L. Y. Jung, and Y. K. Kim, "An organic electrophosphorescent device driven by all-organic thin-film transistor using photoacryl as a gate insulator," *Cur. Appl. Phys.*, vol. 2, pp. 417–419, 2002.
[10] J. Y. Park, H. M. Le, G. T. Kim, H. Park, Y. W. Park, I. N. Kang, D. H. Hwang, and H. K. Shim, "The electroluminescent and photodiode device made of a polymer blend," *Synth. Met.*, vol. 79, pp. 177–181, 1996.
[11] J. Gao, F. Hide, and H. Wang, "Efficient photodetectors and photovoltaic cells from composites of fullerenes and conjugated polymers: Photoinduced electron transfer," *Synth. Met.*, vol. 84, pp. 979–980, 1997.
[12] K. S. Narayan and T. B. Singh, "Nanocrystalline titanium dioxide-dispersed semiconducting polymer photodetectors," *Appl. Phys. Lett.*, vol. 74, pp. 3456–3458, 1999.
[13] G. Yu, Y. Cao, J. Wang, J. McElvain, and A. J. Heeger, "High sensitivity polymer photosensors for image sensing applications," *Synth. Met.*, vol. 102, pp. 904–907, 1999.
[14] G. Yu, G. Srdanov, J. Wang, H. Wang, Y. Cao, and A. J. Heeger, "Large area, full-color, digital image sensors made with semiconducting polymers," *Synth. Met.*, vol. 111–112, pp. 133–137, 2000.
[15] R. Rinaldi, E. Branca, R. Cingolani, S. Masiero, G. P. Spada, and G. Gottarelli, "Photodetectors fabricated from a self-assembly of a deoxyguanosine derivative," *Appl. Phys. Lett.*, vol. 78, pp. 3541–3543, 2001.
[16] N. Camaioni, G. Casalbore-Miceli, M. Catellani, S. Luzzati, and W. Porzio, "Polyalkylthiophene-based photodetector devices: Effect of side-chain length on the device performance," *Mater. Sci. Eng. C*, vol. 15, pp. 261–263, 2001.
[17] R. A. Street, J. Craham, Z. D. Popovic, A. Hor, S. Ready, and J. Ho, "Image sensors combining an organic photoconductor with a-Si:H matrix addressing," *J. Non-Cryst. Sol.*, pp. 1240–1244, 2002.
[18] J. M. Lupton, R. Koeppe, J. G. Müller, J. Feldmann, U. Scherf, and U. Lemmer, "Organic microcavity photodiodes," *Adv. Mater.*, vol. 15, pp. 1471–1474, 2003.
[19] D. Natali, M. Sampietro, M. Arca, C. Denotti, and F. A. Devillanova, "Wavelength-selective organic photodetectors for near-infrared applications based on novel neutral dithiolenes," *Synth. Met.*, vol. 137, pp. 1489–1490, 2003.
[20] S. R. Forrest, "Active optoelectronics using thin-film organic semiconductors," *IEEE J. Select. Topics Quantum Electron.*, vol. 6, pp. 1072–1083, Nov.–Dec. 2000.

[21] P. Peumans, A. Yakimov, and S. R. Forrest, "Small molecular weight organic thin-film photodetectors and solar cells," *J. Appl. Phys.*, vol. 93, pp. 3693–3723, 2003.
[22] D. Natali and M. Sampietro, "Detectors based on organic materials: Status and perspectives," *Nucl. Instrum. Methods A*, vol. 512, pp. 419–426, 2003.
[23] T. Zukawa, S. Naka, H. Okada, and H. Onnagawa, "Organic heterojunction phototransistor," *J. Appl. Phys.*, vol. 91, pp. 1171–1174, 2002.
[24] J. H. Schön and C. Kloc, "Organic metal-semiconductor field-effect phototransistors," *Appl. Phys. Lett.*, vol. 78, pp. 3538–3540, 2001.
[25] K. S. Narayan, A. G. Manoj, T. B. Singh, and A. A. Alagiriswamy, "Novel strategies for polymer based light sensors," *Thin Sol. Films*, vol. 417, pp. 75–77, 2002.
[26] K. S. Narayan and N. Kumar, "Light responsive polymer field-effect transistor," *Appl. Phys. Lett.*, vol. 79, pp. 1891–1893, 2001.
[27] J. D. Gallezot, S. Martin, and J. Kanicki, "Photosensitivity of a-Si:H TFTs," in *Proc. IDRC*, 2001, pp. 407–410.
[28] S. Martin, J. Y. Nahm, and J. Kanicki, "Gate-planarized organic polymer thin-film transistors," *J. Elect. Mater.*, vol. 31, pp. 512–519, 2002.
[29] S. Martin and J. Kanicki, "Organic polymer thin-film transistors for active-matrix flat-panel displays?," in *Proc. IDRC*, 2002, pp. 25–28.
[30] S. Martin, M. C. Hamilton, and J. Kanicki, "Organic polymer thin-film transistors for active-matrix flat-panel displays?," in *SID Tech. Dig.*, vol. 11, 2003, pp. 543–549.
[31] J. H. Lan and J. Kanicki, "Planarized copper gate hydrogenated amorphous-silicon thin-film transistors for AM-LCD's," *IEEE Electron Device Lett.*, vol. 20, pp. 129–131, Mar. 1999.
[32] R. R. Troutman and A. Kotwal, "A device model for the amorphous-silicon staggered-electrode thin-film transistor," *IEEE Trans. Electron Devices*, vol. 36, pp. 2915–2922, Dec. 1989.
[33] R. F. Pierret, *Semiconductor Device Physics*. Reading, MA: Addison-Wesley, 1996.
[34] ——, "Field effect devices," in *Ser. Modular Series on Solid State Devices*, 2nd ed, G. W. Neudeck and R. F. Pierret, Eds. Reading, MA: Addison-Wesley, 1990, vol. IV.
[35] Y. Tsividis, *Operation and Modeling of the MOS Transistor*, 2nd ed. Boston, MA: WCB/McGraw-Hill, 1999.
[36] G. Horowitz and P. Delannoy, "An analytical model for organic-based thin-film transistors," *J. Appl. Phys.*, vol. 70, pp. 469–475, 1991.
[37] A. Rolland, J. Richard, J.-P. Kleider, and D. Mencaraglia, "Electrical properties of amorphous silicon transistors and MIS devices: Comparative study of top nitride and bottom nitride configurations," *J. Electrochem. Soc.*, vol. 149, pp. 3679–3683, 1993.
[38] P. J. Reucroft, "Photocarrier generation mechanisms in polymers," *Photoconductivity in Polymers: An Interdisciplinary Approach*, 1976.
[39] A. R. Brown, C. P. Jarrett, D. M. deLeeuw, and M. Matters, "Field-effect transistors made from solution-processed organic semiconductors," *Synth. Met.*, vol. 88, pp. 37–55, 1997.
[40] M. C. J. M. Vissenberg and M. Matters, "Theory of the field-effect mobility in amorphous organic transistors," *Phil. Rev. B*, vol. 57, pp. 12 964–12 967, 1988.
[41] G. Horowitz, R. Hajlaoui, R. Bourguiga, and M. Hajlaoui, "Theory of the organic field-effect transistor," *Synth. Met.*, vol. 101, pp. 401–404, 1999.
[42] R. E. I. Schropp, A. O. Harm, and J. F. Verwey, "A refined theoretical analysis of photofield-effect measurements in a-Si:H thin-film transistors," *Phil. Mag. B*, vol. 53, pp. 431–444, 1986.
[43] A. O. Harm, R. E. I. Schropp, and J. F. Verwey, "The photofield effect in a-Si:H thin-film MOS transistors: Theory and measurement," *Phil. Mag. B*, vol. 52, pp. 59–70, 1985.
[44] C. van Berkel and M. J. Powell, "Photo-field effect in a-Si:H thin-film transistors," *J. Appl. Phys.*, vol. 60, pp. 1521–1527, 1986.
[45] M. C. Hamilton, S. Martin, and J. Kanicki, "Effect of monochromatic illumination on organic polymer thin-film transistors," in *Proc. IDRC*, 2003, pp. 14–17.
[46] M. C. Hamilton and J. Kanicki, "Organic polymer thin-film transistor photosensors," *IEEE J. Select. Topics Quantum Electron.*, 2004, to be published.
[47] P. Bhattacharya, *Semiconductor Optoelectronic Devices*. Upper Saddle River, NJ: Prentice-Hall, 1997.
[48] G. Fortunato, L. Mariucci, and C. Reita, "Physics of metal/insulator/amorphous semiconductor structures," in *Amorphous & Microcrystalline Semiconductor Devices—Materials and Device Physics*, J. Kanicki, Ed. Norwood, MA: Artech House, 1992.
[49] A. Salleo and R. A. Street, "Light-induced bias stress reversal in polyfluorene thin-film transistors," *J. Appl. Phys.*, vol. 94, pp. 471–479, 2003.

Michael C. Hamilton (S'97) received the B.S. degree in electrical engineering from Auburn University, Auburn, AL, in 2000 and the M.S. degree in electrical engineering from the University of Michigan, Ann Arbor, in 2002, where he is currently pursuing the Ph.D. degree.

Since 2002, he has been a member of the Organic and Molecular Electronics Research Group, Solid State Electronics Laboratory, Department of Electrical Engineering and Computer Science, University of Michigan. His current research interests include organic polymer thin-film electronic and optoelectronic devices.

Sandrine Martin (M'99) received the Ph.D. degree from the University of Paris VI, Paris, France in 1996. She conducted her Ph.D. research on amorphous silicon TFTs for active-matrix liquid crystal displays at the National Center for Telecommunication Studies (CNET), Lannion, France.

She then joined the Center for Display Technology and Manufacturing, University of Michigan, Ann Arbor. Since 1999, she has been a Research Scientist at the Organics and Molecular Electronics Research Group, Department of Electrical Engineering and Computer Science, Solid State Electronics Laboratory, University of Michigan. Her current research interests include organic polymer thin-film devices and circuits, active-matrix flat-panel displays, and application of flat-panel displays to medical imaging.

Jerzy Kanicki (M'99–A'99–SM'00) received the Ph.D. degree in sciences (D.Sc.) from the Universit Libre de Bruxelles, Brussels, Belgium, in 1982.

He subsequently joined the IBM Thomas J. Watson Research Center, Yorktown Heights, NY, as a Research Staff Member, working on hydrogenated amorphous silicon devices for the photovoltaic and flat-panel display applications. In 1994, he moved from IBM Research Division to the University of Michigan, Ann Arbor, as a Professor in the Department of Electrical Engineering and Computer Science (EECS). His research interests within the Electrical and Computer Engineering (ECE) division of the EECS, include organic and molecular electronics, TFTs and circuits, and flat-panel displays technology, including organic light-emitting devices.